JNeurosci
THE JOURNAL OF NEUROSCIENCE

Research Articles: Systems/Circuits

Echoes from intrinsic connectivity networks in the subcortex

https://doi.org/10.1523/JNEUROSCI.1020-23.2023

Cite as: J. Neurosci 2023; 10.1523/JNEUROSCI.1020-23.2023

Received: 1 June 2023
Revised: 11 July 2023
Accepted: 28 July 2023

Echoes from intrinsic connectivity networks in the subcortex

Abbreviated title: Echoes in the subcortex

Josephine M Groot[1,2], Steven Miletic[2], Scott JS Isherwood[2], Desmond HY Tse[3], Sarah Habli[4], Asta K Håberg[5,6], Birte U Forstmann[2], Pierre-Louis Bazin[1,7]*, Matthias Mittner[1]*

*Authors contributed equally

[1] Department of Psychology, UiT – The Arctic University of Norway, 9037 Tromsø, Norway
[2] Integrative Model-based Cognitive Neuroscience research unit, University of Amsterdam, 1001 NK Amsterdam, The Netherlands
[3] Department of Neuropsychology and Psychopharmacology, Maastricht University, 6200 MD Maastricht, The Netherlands
[4] Department of Psychology, Norwegian University of Science and Technology, 8900 Trondheim, Norway
[5] Department of Neuromedicine and Movement Science, Norwegian University of Science and Technology, 8900 Trondheim, Norway
[6] Department of Radiology and Nuclear Medicine, St. Olavs Hospital, 7006 Trondheim, Norway
[7] Departments of Neurophysics and Neurology, Max Planck Institute for Human Cognitive and Brain Sciences, 04303 Leipzig, Germany

Corresponding author: matthias.mittner@uit.no

Number of pages:	33
Number of figures/tables:	4/1
Words abstract:	229
Words Introduction:	658
Words Discussion:	1637

Funding
This work was financially supported by the Netherlands Organization of Scientific Research (NWO; grant number 016.Vici.185.052 to BUF).

Abstract

Decades of research have greatly improved our understanding of intrinsic human brain organization in terms of functional networks and the transmodal hubs within the cortex at which they converge. However, substrates of multi-network integration in the human subcortex are relatively uncharted. Here, we leveraged recent advances in subcortical atlasing and ultra-high field (7T) imaging optimized for the subcortex to investigate the functional architecture of fourteen individual structures in healthy adult males and females with a fully data-driven approach. We revealed that spontaneous neural activity in subcortical regions can be decomposed into multiple independent subsignals that correlate with, or 'echo', the activity in functional networks across the cortex. Distinct subregions of the thalamus, striatum, claustrum, and hippocampus showed a varied pattern of echoes from attention, control, visual, somatomotor, and default mode networks, demonstrating evidence for a heterogeneous organization supportive of functional integration. Multiple network activity furthermore converged within the globus pallidus externa, substantia nigra, and ventral tegmental area but was specific to one subregion, while the amygdala and pedunculopontine nucleus preferentially affiliated with a single network, showing a more homogeneous topography. Subregional connectivity of the globus pallidus interna, subthalamic nucleus, red nucleus, periaqueductal grey, and locus coeruleus did not resemble patterns of cortical network activity. Together, these finding describe potential mechanisms through which the subcortex participates in integrated and segregated information processing and shapes the spontaneous cognitive dynamics during rest.

Keywords: resting-state, 7 Tesla, functional connectivity, dual regression, network integration

Significance statement

Despite the impact of subcortical dysfunction on brain health and cognition, large-scale functional mapping of subcortical structures severely lags behind that of the cortex. Recent developments in subcortical atlasing and imaging at ultra-high field provide new avenues for studying the intricate functional architecture of the human subcortex. With a fully data-driven analysis, we reveal subregional connectivity profiles of a large set of non-cortical structures, including those rarely studied in fMRI research. The results have implications for understanding how the functional organization of the subcortex facilitates integrative processing through cross-network information convergence, paving the way for future work aimed at improving our knowledge of subcortical contributions to intrinsic brain dynamics and spontaneous cognition.

Introduction

A large body of research in the past decades has focused on descriptions of the macroscopic organization of the human brain in terms of intrinsic functional connectivity (FC) and its role in orchestrating cognition and behavior (Damoiseaux et al 2006; Liégeois et al 2019; Lee et al 2019). The integration of distributed, functionally specialized brain networks is thought to be essential, especially for higher-level cognition and consciousness (Senden et al 2014; Bell and Shine 2016). With a variety of methods, specific sites for network convergence have been identified in the posterior cingulate cortex (PCC), anterior cingulate cortex (ACC), and the posterior parietal cortices (Tomasi and Volkow 2011; Bell and Shine 2015; Lyu et al 2021), revealing an ensemble of transmodal regions in the cortex that enable efficient global communication (Van der Heuvel and Sporns 2011; Grayson et al 2014). With a novel multivariate approach, it was revealed that subtle signals from functionally specialized subdivisions within these regions have connectivity profiles that mirror, or 'echo', the activity of different networks, potentially indicating a mechanism through which they facilitate cross-network information integration (Leech et al 2012; Braga et al 2013; Braga & Leech 2015).

Although this work has provided important insights, the dominating corticocentric view overlooks potential contributions from the highly diverse and interconnected structures in the subcortex (Bell and Shine 2016; Forstmann et al 2017; Tian et al 2020). This knowledge gap is likely related to the challenges associated with visualizing the subcortex using conventional MRI due to the varied magnetic tissue properties and generally weaker signal-to-noise ratio (SNR) compared to the cortex (De Hollander et al 2017; Keuken et al 2018). Nonetheless, many subcortical structures are part of extensive cortico-subcortical circuitry and demonstrate widespread FC to networks including the default mode network (Haber 2003; Bär et al 2016; Lee et al 2018; Ji et al 2019; Li et al 2021). Compared to the smaller subcortical nuclei in the deep brain, larger structures such as the thalamus and striatum have received a relatively high amount of attention, establishing their hub-like properties and roles in integrative processing (Choi et al 2012; Jarbo and Verstynen 2015; Hwang et al 2017; Seitzman et al 2020; Greene et al 2020; Cheng and Liu 2021). However, most of the

subcortex remains underrepresented in human functional MRI (fMRI) studies and the majority of available evidence is based on lower field strength (3 Tesla), often combined with extensive spatial smoothing, both of which limit the spatial resolution needed to resolve smaller nuclei and increase the risk for signal blurring (De Hollander et al 2015; Forstmann et al 2017).

Due to these shortcomings, the functional architecture of the subcortex and its role in integrative processing remains poorly understood. Given that subcortical dysfunction is heavily implicated in a wide range of neuropsychiatric diseases, advancing this knowledge may be vital for our understanding of healthy cognitive functioning as well as improving disease models. Charting the topography of network echoes within the subcortex provides a compelling approach to accomplish new insights into the subcortical contributions to whole-brain communication and higher-level cognition. Following previous work (Leech et al 2012; Braga et al 2013), we define an echo as a unique subregional connectivity profile that traces the activity pattern of a functional network. By leveraging recent advances in automated parcellation algorithms and sensitive fMRI protocols for the subcortex at ultra-high field (Bazin et al 2020; Miletic et al 2020), we aim to extend the previously established multivariate echo analysis to a large set of subcortical structures, including those rarely studied with human fMRI: the thalamus, striatum, globus pallidus externa, globus pallidus interna, subthalamic nucleus, claustrum, hippocampus, amygdala, substantia nigra, red nucleus, ventral tegmental area, locus coeruleus, periaqueductal grey, and pedunculopontine nucleus. Similar to findings for the cortex, we expect that subcortical structures organized to facilitate multi-network integration demonstrate a heterogeneous subregional topography of intrinsic echoes from separate functional networks, which are likely hidden with previous univariate connectivity analyses.

Methods

Participants

The study was approved by the Ethics Review Board of the University of Amsterdam and the Regional Committees for Medical and Health Research Ethics in Norway. Forty healthy adults between 19 and 39 years old (21 female, mean age=26.5, *SD*=5.5 years) were recruited from the general population in Norway and screened for MRI compatibility. Exclusion criteria were self-reported (history of) neurological or psychiatric disease, impaired vision, or any contra-indications for MRI such as metal implants. Written informed consent was obtained from all participants prior to data collection. All materials, code, and unthresholded group-level statistical maps from multivariate as well as (supplementary) univariate connectivity analyses are publicly available in an Open Science Framework repository at https://osf.io/wt3uc.

fMRI acquisition and preprocessing

Neuroimaging data were collected with a Siemens MAGNETOM Terra 7 Tesla (7T) system with a 32-channel phased-array head coil. Structural images were obtained with a MP2RAGE sequence (Marques et al 2010) in 224 sagittal slices at 0.75mm isotropic voxel resolution (TR=4300ms; $TI_{1,2}$=840, 2370ms; flip-angles$_{1,2}$=5, 6^{o}; TE=1.99ms; FOV=240×240×168mm). Functional images were acquired using a gradient echo echo-planar imaging (EPI) sequence with a voxel resolution of 1.5mm isotropic (82 transverse slices per volume; TR=1380ms; TE=14ms; flip-angle=60^{o}; in-plane acceleration factor (GRAPPA)=3; multiband acceleration factor=2; partial Fourier=6/8). An additional EPI sequence with opposite phase-encoding direction was performed for susceptibility distortion correction purposes. Heart rate and respiratory data were acquired with a fingerclip and waistband, respectively, to correct for physiological noise, which is especially prominent in the subcortex.

MR images were preprocessed with fMRIPrep (v20.2.6; Esteban et al 2018) in the Nipype framework (Gorgolewski et al 2011). The structural (T1-weighted) scan was corrected for intensity non-uniformity with N4BiasFieldCorrection (ANTs v2.3.3; Tustison et al 2010) and skull-stripped with

antsBrainExtraction using the OASIS30ANTs target template. Brain tissue segmentation of cerebrospinal fluid (CSF), white matter (WM), and gray matter (GM) was performed with FAST (FSL v5.0.9; Zhang et al 2001). For each of the two resting-state runs, a reference volume and its skull-stripped version were generated. A fieldmap based on the EPI references with opposing phase-encoding directions was calculated with 3dQwarp (AFNI; Cox 1996) and susceptibility distortion correction was applied to the EPI reference prior to co-registration to the T1-weighted reference using the boundary-based registration cost-function in bbregister with 6 degrees of freedom (FreeSurfer; Greve and Fischl 2009). Head-motion parameters (rotation and translation) were estimated with MCFLIRT (FSL v5.0.9; Jenkinson et al 2002) and slice-time correction to half of the acquisition range (0.674s) was performed with AFNI's 3dTshift. Following fMRIPrep, data were spatially smoothed with a full-width half-maximum Gaussian kernel of 1.5mm using SUSAN (Smith and Brady 1997) and denoised with a first-level general linear model in FEAT (Woolrich et al 2001) that included fMRIPrep-derived confound regressors, including: mean signal in CSF and WM, framewise displacement (FD), six rotation and translation parameters, and discrete-cosine transform (DCT) basis functions to model low-frequency scanner drifts. In addition, cardiac and respiratory sources of nuisance were based on acquired physiological data and modeled with RETROICOR (Glover et al 2000) using the Matlab PhysIO toolbox (Kasper et al 2017) in TAPAS (Frässle et al 2021). For one subject with missing physiological data, the same number of fMRIPRrep's anatomical component-based noise correction (aCompCor; Behzadi et al 2007) regressors were entered in the model instead. The modeled data were obtained via linear regression and normalized. Finally, the two residual runs were concatenated and registered to the ICBM 152 Nonlinear Assymetrical template version 2009c (MNI152Nlin2009cAsym; Fonov et al 2009) using the nonlinear registration tool in antsRegistration (Avants et al 2008) with the transformation parameters provided by fMRIPrep.

Table 1. Parcellation details for regions of interest (ROIs)

		N voxels	Mean (SD) tSNR	Source
Forebrain				
Thalamus	Tha	6130	47.94 (6.31)	MASSP
Striatum	Str	8552	52.17 (8.11)	MASSP
Globus pallidus externa	GPe	1241	35.44 (5.58)	MASSP
Globus pallidus interna	GPi	453	34.18 (4.39)	MASSP
Subthalamic nucleus	STN	93	32.30 (4.25)	MASSP
Claustrum	Cl	683	59.12 (4.71)	MASSP
Hippocampus	HPC	2894	37.84 (10.44)	17-network cortical parcellation
Amygdala	Amg	1063	39.89 (7.22)	MASSP
Midbrain				
Substantia nigra	SN	481	31.51 (5.32)	MASSP
Red nucleus	RN	232	33.75 (3.05)	MASSP
Ventral tegmental area	VTA	220	37.68 (3.05)	MASSP
Periaqueductal grey	PAG	198	32.37 (10.56)	MASSP
Brainstem				
Locus coeruleus	LC	98	39.01 (7.31)	7T Probabilistic LC Atlas
Pedunculopontine nucleus	PPN	135	40.00 (3.29)	MASSP

Experimental design and regions of interest

Two runs of 15 minutes eyes-open wakeful rest (fixation on centered cross) were collected together with anatomical scans during the first of four sessions that were part of a larger multi-session 7T study. The anatomical and experimental data acquired during the other sessions are not part of this study. Figure 1 provides an overview of the analysis, extending the data-driven echo approach (Leech et al 2012; Braga et al 2013) to the subcortex. With this multivariate technique, unique FC patterns are estimated while controlling for other subsignals within a region, revealing a more subtle subregional functional organization beyond a region's global connectivity profile that remains concealed with univariate analyses (Leech et al 2012).

Fourteen subcortical regions of interest (ROIs) were defined based on open-source parcellations (Table 1, Figure 2a). Binary ROI masks were computed from the Multi-contrast Anatomical Subcortical Parcellation algorithm (MASSP; Bazin et al 2020) that is based on quantitative MRI data (*N*=105, ages 18-80) from the 7T Amsterdam ultra-high field adult lifespan database (AHEAD; Alkemade et al 2020) in high-resolution MNI space (MNI152Nlin2009bAsym; Fonov et al 2009). The

MASSP parcellations include the thalamus (Tha), striatum (Str), claustrum (Cl), globus pallidus externa (GPe), globus pallidus interna (GPi), substantia nigra (SN), subthalamic nucleus (STN), ventral tegmental area (VTA), red nucleus (RN), amygdala (Amg), periaqueductal grey (PAG), and pedunculopontine nucleus (PPN). The locus coeruleus (LC) was defined with the 7T Probabilistic LC Atlas based on 53 healthy adults aged 52-84 years (Ye et al 2021). In addition, the 17-network cortical parcellation (Yeo et al 2011) was used for extracting a mask of the hippocampus (HPC), which was taken from the Default C network. To validate the results for non-cortical structures, we also assessed if we could reproduce the pattern of echoes within various cortical regions, including the PCC, medial prefrontal cortex (mPFC), and visual cortex (Braga et al 2013). We used the same cortical network parcellation to derive masks for the striate and extrastriate cortex (Visual Central network) and the PCC and mPFC (Default A network). For bilateral ROIs, left and right hemispheres were combined into a single binary mask and all masks were resampled to the resolution of the functional data with FLIRT using nearest-neighbor interpolation (v6.0; Jenkinson and Smith 2001). The probabilistic LC mask was thresholded liberally so that voxels that overlapped 1% or more were included in the resampled mask.

Statistical analysis

The individual preprocessed resting-state timeseries were masked with each of the binary ROIs and decomposed into 10 spatiotemporal independent subregions with a spatially-restricted group canonical independent component analysis (canICA) as implemented in Nilearn. Although the temporal concatenation ICA approach is a popular technique in combination with dual regression, biases in the estimation of group-level networks may arise with varying degrees of inter-individual variability (Hu and Yang 2021). Instead, canICA applies a hierarchical approach in which individual data is decomposed prior to canonical correlation analysis to identify group commonalities (Varoquaux et al 2010). The ROI-wise canICA's were restricted to find 10 independent components. Model order selection constitutes a main challenge in ICA, and the exact number of underlying

signals in the diverse subcortical structures remains unknown. While prior analyses on the PCC demonstrated qualitatively similar outcomes for various model orders (Leech et al 2012), conducting such comprehensive comparisons for all included structures was beyond the scope of this study. Instead, we opted to follow previous approaches and fix the number of components, addressing interregional differences in network echoes rather than precise dimensionality of individual structures.

Following spatiotemporal decomposition, the unique whole-brain FC of each independent component (subregion) was then investigated with dual regression (Beckmann et al 2009; Zuo et al 2010). First, the 10 spatial maps from the canICA were regressed onto every individual's whole-brain resting-state data to estimate the subject-specific timecourse for each subregion. By simultaneously entering all 10 spatial maps as design matrix, the timecourse for each subregion was estimated while statistically controlling for the variance in the other subregions' timecourses. Second, the 10 subject-specific independent timecourses were regressed onto the subject's resting-state data to obtain spatial maps corresponding to the whole-brain, voxel-wise unique FC of each subregion. These subject-level FC maps were then combined in a non-parametric group-level analysis using random permutation testing (5000 permutations) with threshold-free cluster enhancement (TFCE). This resulted in one group-level *t*-statistical map for each of the 10 subregions within each individual ROI that was thresholded with family-wise error (FWE) correction at $p<.05$.

To quantify the presence of echoes from canonical resting-state networks within subcortical regions, the thresholded group-level FC maps were spatially correlated with data-driven reference networks obtained from a canICA on the whole-brain timeseries restricted to find 20 independent components. Based on visual inspection and low spatial Pearson product-moment correlation coefficients with an established 17-network cortical parcellation (Yeo et al 2011), four independent components ($r=.05$, $r=.04$, $r=.13$, $r=.04$) were identified as artifactual and removed from further analysis. The resulting 16 reference networks were masked with the cortical network parcellation to remove any voxels located outside cortical grey matter (e.g., cerebral white matter, subcortex, CSF).

236 The extent of the spatial correlation between the FC map for each subregion and the reference
237 networks was used to identify whether patterns of cortical network activity were mirrored, or
238 echoed, in the unique subregional timecourses.

Results

Data-driven networks correspond to existing cortical network parcellations

The 16 data-driven reference networks were labeled automatically according to their maximum spatial correlation with the well-established 17-network cortical parcellation (Yeo et al 2011; Figure 2b), which is based on rs-fMRI data from 1000 individuals. Despite large differences in field strength, data resolution, and parcellation method, we found correlation coefficients ranging from 0.21 to 0.67 (mean r=.44, SD=.14), generally indicating moderate to good spatial overlap with their reference network counterparts (Figure 2b, lower right): Somatomotor A (r=.66), Somatomotor B (r=.30), Control A (r=.46), Control B (r=.51), Control C (r=.57), Salience/Ventral Attention A (r=.34), Salience/Ventral Attention B (r=.54), Temporal Parietal (r=.21), Dorsal Attention A (r=.46), Dorsal Attention B (r=.25), Default A (r=.42), Default B (r=.47), Limbic A (r=.30), Limbic B (r=.41), Visual Central (r=.49), and Visual Peripheral (r=.67). The data-driven Temporal Parietal network also partially overlapped with the Control A network parcellation (r=.15).

Together, the reference networks covered 66% of cortical grey matter defined in the parcellation by Yeo et al (2011). The strongest deviation was observed in the anterior temporal cortex, which was not remedied by increasing model order (40 or 100 independent components) or a cortically-restricted canICA. To assess corresponding variations in temporal SNR (tSNR), we calculated voxel-wise tSNR values as the ratio of the mean and standard deviation of the resting-state timeseries after temporal high-pass filtering (1/128s). Individual tSNR maps were registered to standard MNI space and averaged (voxel-wise) across subjects and runs. Compared to other cortical areas, reduced tSNR in the temporal lobe was observed, and as a consequence, temporal networks were underrepresented in the analysis (Figure 2-1).

Subcortical structures echo signals from different resting-state networks

The 10 thresholded FC maps for each ROI, representing the unique whole-brain FC of each subregion at the group-level, were spatially correlated with the 16 unthresholded spatial maps of the

data-driven reference networks. Figure 3a summarizes the degree of network echoes for the nine ROIs that demonstrated at least one spatial correlation with any reference network above a threshold that was arbitrarily set at the 97th percentile of all spatial correlations (r=0.16). Echoes were summarized by counting above-threshold spatial correlations in terms of (1) the number of reference networks represented in each ROI and (2) the number of subregions that echoed a reference network. For example, six distinct striatal subregions displayed FC profiles that spatially correlated above-threshold with in total 10 different resting-state networks. Figure 3b presents the actual maximum spatial correlations between each ROI and each reference network, independent of subregion. The reference network that was represented most often was the Salience B network, correlating above-threshold with seven ROIs, followed by Default A, Control C, and Visual Peripheral, each with at least one above-threshold spatial correlation with six different ROIs.

Seven subcortical ROIs echoed signals from more than one network, including: the thalamus (Tha), striatum (Str), hippocampus (HPC), claustrum (Cl), globus pallidus externa (GPe), substantia nigra (SN), and ventral tegmental area (VTA). The former four ROIs furthermore showed that the echoes from different reference networks were distributed among multiple subregions, indicating evidence for a heterogeneous functional organization. In contrast, both the amygdala (Amg) and pedunculopontine nucleus (PPN) showed medium and small spatial correlations, respectively, with only one reference network (Amg: r=.37 [DefA]; PPN: r=.19 [SalB]). The globus pallidus interna (GPi), subthalamic nucleus (STN), red nucleus (RN), periaqueductal grey (PAG), and locus coeruleus (LC) failed to show evidence of echoes as none of their subregions demonstrated a connectivity pattern that resembled the pattern of an intrinsic connectivity network. In some cases, a subregion's FC profile was widespread and shared spatial similarity with more than one reference network. Figure 3-1 presents a few FC maps to illustrate the diversity and similarity in connectivity profiles to different reference networks across a subset of subcortical structures.

The FC maps of each subregion were also spatially correlated with the 17-network cortical parcellation (Yeo et al 2011), which yielded generally lower spatial correlations but a qualitatively

similar pattern of results (Figure 3-2). To validate these novel results for the subcortex, we repeated the analyses for three cortical regions that were previously investigated. Results for the PCC, mPFC, and visual cortex are presented in Figure 3-3 and are largely consistent with previous findings (Leech et al 2012; Braga et al 2013).

Topographic organization of functionally heterogeneous subcortical structures

Figure 4 shows the topographic pattern of network echoes in the subregions of the seven ROIs with more than one above-threshold spatial correlation. Subregions are color coded according to the reference network they echoed most strongly, whereas subregions with a maximum spatial correlation below threshold (r<0.16) are translucent. For every ROI, there were several subregions that did not mirror the activity in any intrinsic connectivity network, because they were predominantly functionally connected to other subcortical structures or because their signal largely reflected noise upon visual inspection.

Five thalamic subregions echoed signals from various reference networks, demonstrating a heterogeneous organization that was mostly symmetrically distributed in bilateral subdivisions. Left and right ventromedial subregions were both most strongly correlated to the Somatomotor A network (left: r=.26, right: r=.20), although the right subregion's connectivity profile also spatially overlapped with Salience B (r=.20). A more dorsomedial bilateral subregion displayed a connectivity pattern that correlated with the pattern of multiple reference networks, including Default A (r=.38), Default B (r=.32), and Control A (r=.25). Another bilateral subregion, more dorsolaterally located, correlated most strongly with the Dorsal Attention A network (r=.31), although there was also spatial overlap with Somatomotor A (r=.29), Dorsal Attention B (r=.25), and Visual Peripheral (r=.24) networks. Finally, the Default B network was represented in the posterior part of the left-sided thalamus (r=.22).

Within the striatum, there were six different subregions that echoed one or more reference networks, located mostly within the caudate nucleus. A subregion primarily in the left tail of the

caudate nucleus spatially correlated with the Default B network (*r*=.21), whereas a subregion covering more of the right tail of caudate nucleus most strongly echoed Control B (*r*=.26), although its widespread connectivity pattern also overlapped with Temporal Parietal (*r*=.23) and Salience A (*r*=.22) networks. A bilateral subregion covering the nucleus accumbens correlated most strongly with Default A (*r*=.40), whereas another bilateral subregion in the mediodorsal part of the caudate head was functionally connected with Control A (*r*=.26) and Default B (*r*=.21) networks. Subregions that most strongly echoed the Salience A network included a division in the posterior parts of the left caudate tail and left putamen (*r*=.20) as well as a bilateral region in the lateral nucleus accumbens (*r*=.19).

For the hippocampus, we observed that different intrinsic connectivity networks were echoed within four different subregions. In the left hemisphere, a posterior dorsal subregion correlated most strongly with Default A (*r*=.34), whereas a more ventrally located subregion correlated exclusively with the Limbic A network (*r*=.24). A bilateral anteromedial subregion was functionally connected to the Visual Central network (*r*=.21), whereas a posterior dorsal subregion in the right hemisphere echoed the Visual Peripheral (*r*=.30) as well as the Dorsal Attention networks (DorA: *r*=.28, DorB: *r*=.30).

Five subregions of the claustrum showed an FC profile that correlated with different reference networks. A small, bilateral subregion in the ventral claustrum had a widespread cortical connectivity that had the strongest spatial similarity with Dorsal Attention A (*r*=.23), but also Somatomotor A (*r*=.20), Dorsal attention B (*r*=.19), and Salience B (*r*=.19) networks. Left and right subdivisions in the posterior part both echoed the Salience A network (*r*=.26 and *r*=.21, respectively). In addition, an exclusive functional connection with the Default B network was observed in an anterior subregion of the left claustrum (*r*=.32) and with the Somatomotor A network in a more posterior subregion of the right claustrum (*r*=.35).

The GPe and SN each had one subregion with a widespread connectivity profile comprising seven and three reference networks, respectively (Figure 3b). In the GPe, a bilateral dorsolateral

subdivision most strongly echoed the Somatomotor A network (*r*=.26), but its signal also correlated with activity in Dorsal Attention A (*r*=.23) and Control networks A and B (*r*=.20 and *r*=.22, respectively). The most pronounced network echo within the SN was from Default A (*r*=.24) and came from a bilateral subregion in the medial anterior SN. The same subregion also showed traces from Salience B (*r*=.22) and Control C (*r*=.16) networks. For the VTA, a large inferomedial subdivision in the right hemisphere was most strongly connected to Salience B (*r*=.19) and just below threshold to Visual Peripheral (*r*=.15) networks. Echoes from the Default A network were furthermore present in two other subregions of the VTA, but spatial correlations were weaker (*r*=.15 and *r*=.13).

Discussion

Despite accumulating insights into the mechanisms of functional integration within the cortex, subcortical substrates of cross-network convergence are largely unexplored. Nonetheless, the subcortex is embedded within an extensive cortico-subcortical architecture that is thought to serve integrative rather than purely segregated functions (Haber 2003). Here, we aimed to more closely examine the underlying functional organization of subcortical nuclei and their subregional connectivity to functional networks across the cortex.

Consistent with our expectations, we show that individual subcortical structures contain a composite of neural signals that can be decomposed into activity traces of intrinsic network activity. In their study, Braga et al (2013) showed that activity in multiple networks converges at specific transmodal zones in the cortex, as reflected in a mixture of signals that partially correlate with different networks. We demonstrate that this property is not limited to cortical regions by revealing potential mechanisms for multi-network integration in the subcortex. The results provide the strongest evidence for functional heterogeneity within the thalamus, striatum, claustrum, and hippocampus, for which we observed a complex pattern of subregional whole-brain FC that resembled spontaneous activity in distinct functional networks. Subregions in left and right hemispheres had similar spatiotemporal signatures that echoed the same functional networks, showing a symmetrical bilateral topography that is consistent with prior work (Cheng and Liu 2021).

The thalamus and striatum are the most commonly represented non-cortical structures in studies of global brain connectivity, providing support for their putative role as hub regions (Bell and Shine 2015, 2016; Van der Heuvel and Sporns 2011). Whereas several studies report an amalgamation of primarily sensory information within thalamic subregions consistent with its gating function (Tomasi and Volkow 2011; Ji et al 2019), we observed traces of somatomotor as well as default mode and dorsal attention networks. The somatomotor subdivisions also spatially overlapped with cingulo-opercular regions of the salience network, which aligns with findings of a ‘motor integration zone’ within ventral thalamic nuclei (Greene et al 2020). Additionally, dorsal attention, somatomotor, and

visual networks converged in a dorsolateral subregion, similar albeit slightly less posterior to the 'visual integration zone' in the pulvinar nucleus reported earlier (Greene et al 2020). For the striatum, we observed signal echoes from default mode, control, and salience networks predominantly within the caudate head and left tail, right tail, and left putamen, respectively. Despite large methodological differences across studies, these findings are consistent with prior evidence for 'cognitive' integration within the striatum (Choi et al 2012; Greene et al 2020; Seitzman et al 2020) and supports thalamic and striatal roles in information integration and higher-level cognitive functioning (Haber, 2003; Hwang et al 2017).

Although organizational principles may broadly concur, precise functional boundaries and network connections diverge across studies. For example, the subregional profiles identified here partially deviate from another data-driven co-partitioning (Cheng and Liu 2021) and a voxel-wise winner-take-all approach (Seitzman et al 2020) for the thalamus, as well as the from the striatal architecture reported by Choi et al (2012). Additionally, we found inter-hemispheric differences in the hippocampus – i.e., visual and dorsal attention network echoes in the right and default mode and limbic in the left side – that are inconsistent with reports of lateralized subdivisions along an anterior-posterior axis, as well as the location along this axis of the preferential connection to the default mode network (Blessing et al 2016; Cheng et al 2020; Ezama et al 2021). Given differences in connectivity with entorhinal and parahippocampal cortex (Qin et al 2016; Seoane et al 2018), it is possible that the extent of hippocampal and surrounding voxels included in the analysis explains some of the discrepancies across studies, which might be further exacerbated by the effects of spatial smoothing. Furthermore, high degrees of individual variability in subcortical anatomy and functional connectivity may result in distortions of group-level estimations (De Hollander et al 2015; Sylvester et al 2020; Greene et al 2020; Tian et al 2020; Marek and Greene 2021).

Similar to previous observations for the cortex (Braga et al 2013), we demonstrate that functional heterogeneity is not ubiquitously present throughout the subcortex. Within the GPe, SN, and VTA, only one subregion's connectivity profile resembled patterns of functional network activity. A region

403 in the dorsolateral GPe echoed somatomotor as well as dorsal attention and control networks,
404 indicating an integrative site that may support its known role in voluntary, planned movement. Both
405 the SN and VTA showed a pattern of converging signals from default mode and salience networks,
406 although less evident in the VTA. Whereas this association with the default mode network is more
407 established (Bär et al 2016; Edlow 2021; Zhang et al 2016; Li et al 2021), connectivity to the salience
408 network is less known and may indicate involvement in attention and spontaneous cognition
409 (O'Callaghan et al 2020).

410 No clear evidence for functional integration was observed for the amygdala and PPN. Whereas
411 the PPN likely takes part in more specialized subcortical circuitry involved in arousal and locomotion
412 (Martinez-Gonzales et al 2011; Bennarroch 2013), the amygdala was previously proposed as hub
413 structure (Tomasi and Volkow 2011) and showed dissociable FC profiles from its separate nuclei
414 (Kerestes et al 2017). Although we did not find evidence for such heterogeneity when controlling for
415 other subregional timecourses, we observed an intact connection with the default mode network,
416 which is supported by other work (Kerestes et al 2017; Sylvester et al 2020; Harrison et al 2021). For
417 the remaining structures – i.e., GPi, STN, RN, PAG, and LC – we failed to find network echoes.
418 Although previous univariate FC studies have indicated correlations with widespread cortical activity
419 for some of these structures (e.g., Zhang et al 2016; Anteraper et al 2018), the multivariate analysis
420 here did not result in a clear group-level pattern of cortical connectivity. Similar to the PPN, these
421 structures may be less involved in integrating spontaneous signals from distributed functional
422 processes across the cortex, but are likely more strongly embedded in local networks to support
423 segregated functional processing (Singh et al 2022). Recent findings suggest that neuromodulatory
424 nuclei for dopaminergic and noradrenergic systems are driving systems-level integration and
425 cognition (Liu et al 2017; De Gee 2017; Zhang et al 2016). However, not all findings converge. For
426 example, Bär et al (2016) showed that LC connectivity to the default mode network disappeared
427 when controlling for adjacent neural signals and that hub-like features of midbrain nuclei were not
428 supported by a graph theory analysis. The results presented here align with this observation and

emphasize that integrative properties of these structures, among which the LC, remain somewhat elusive. Given proposed roles of the LC in mediating the dynamics of cortical connectivity and neural gain (Aston-Jones & Cohen 2005; Munn et al 2021), it is perhaps not surprising that no dissociable traces of functional network activity are observed. That is, the LC may drive global states of network integration and segregation rather than serving as a convergence zone in itself.

In summary, our results suggest that subcortical structures exhibit varying degrees of functional heterogeneity. This characteristic might be expressed along a gradient, where structures adjacent to the cortex seem more likely to support multi-network integration compared to deep brain nuclei. However, several factors may confound interpretations of interregional differences in the subcortex. For example, deep brain nuclei are generally smaller in size and have weaker SNR, while subcortex near the cortex is susceptible to signal bleeding from adjacent cortical voxels, to which they are also reciprocally connected (Choi et al 2012). This issue might be especially prominent in the claustrum, which is a thin sheet-like structure situated directly between the striatum and insula. In a recent study, Krimmel et al (2019) used a novel regression technique on similar high-resolution fMRI data (1.5mm isotropic voxels) to isolate the signal in the claustrum from nearby cortical and striatal voxels, which preserved the widespread FC with cortical networks involved in attention and cognitive control. Even though we did not correct for potential signal bleeding beyond limiting the amount of spatial smoothing, our finding of functionally heterogeneous network echoes within the claustrum's subdivisions coincides with this work and its postulated role in attention and cognition (Bell and Shine 2015; Krimmel et al 2019; Smith et al 2020).

It should be noted that recent work highlights the difference in FC between eyes-open and eyes-closed resting-state conditions, particularly with regard to internetwork connectivity of visual and sensorimotor networks to default mode and salience networks (Agcaoglu et al 2019; Costumero et al 2020; Han et al 2023). While a large portion of studies on subcortical connectivity cited here are correspondingly based on eyes-open resting-state fMRI (e.g., Greene et al 2020; Choi et al 2012; Seitzman et al 2020; Hwang et al 2017; Blessing et al 2016; Sylvester et al 2020), future efforts could

contrast our results to potential reconfigurations during other resting-state and experimental conditions. Investigating changes in the pattern of echoes according to external factors, such as cognitive demand, and internal state are likely necessary to illuminate their functional relevance (e.g., Leech et al 2012).

Although the precise significance of network echoes for cognition and behavior is not resolved, we strengthen the evidence that the subcortex participates in cross-network integration through echoing intrinsic network activity. These results may ignite new intriguing hypotheses on the mechanisms of spontaneous cognitive processes such as mind wandering (Mittner et al 2016; Zuberer et al 2021). Previous work has shown that mind wandering correlates with activity and connectivity in the default mode and frontoparietal control networks as well as the subcortex (Mittner et al 2014; Kucyi et al 2017; Groot et al 2022). Given that both subtle and pronounced reorganizations in FC occur with changes in task demand (Leech et al 2012; Braga et al 2013; Tian et al 2020), investigations of how the complex pattern of echoes in the subcortex is perturbed by attentional changes may reveal novel insights into the mechanisms that drive mind wandering.

References

Agcaoglu O, Wilson TW, Wang Y-P, Stephen J, Calhoun VD (2019) Resting state connectivity differences in eyes open versus eyes closed conditions. *Hum Brain Map,* 40:2488-2498. doi: 10.1002/hbm.24539

Alkemade A, Mulder MJ, Groot JM, Isaacs BR, Van Berendonk N, Lute N, Isherwood SJS, Bazin P-L, Forstmann BU (2020) The Amsterdam Ultra-high field adult lifespan database (AHEAD): A freely available multimodal 7 Tesla submillimeter magnetic resonance imaging database. *NeuroImage, 221*:117200. doi: 10.1016/j.neuroimage.2020.117200

Anteraper SA, Guell X, Whitfield-Gabrieli S, Triantafyllou C, Mattfeld AT, Gabrieli JD, Geddes MR (2018) Resting-state functional connectivity of the subthalamic nucleus to limbic, associative, and motor networks. *Brain Connectivity, 8:*22-32. doi: 10.1089/brain.2017.0535

Aston-Jones G, Cohen JD (2005) An integrative theory of locus coeruleus-norepinephrine function: Adaptive gain and optimal performance. *Annu Rev Neurosci*, 28:403-450. doi: 10.1146/annurev.neuro.28.061604.135709

Avants B, Tustison NJ, Song G (2008) Advanced normalization tools (ANTS). *Insight Journal,* 1-35. doi: 10.54294/uvnhin.

Bär K-J, De la Cruz F, Schumann A, Koehler S, Sauer H, Critchley H, Wagner G (2016) Functional connectivity and network analysis of midbrain and brainstem nuclei. *NeuroImage, 134:*53-63. doi: 10.1016/j.neuroimage.2016.03.071

Bazin P-L, Alkemade A, Mulder MJ, Henry AG, Forstmann BU (2020) Multi-contrast anatomical subcortical structures parcellation. *eLife, 9:*e59430. doi: 10.7554/eLife.59430

Beckmann CF, Mackay CE, Filippini N, Smith SM (2009) Group comparison of resting-state fMRI data using multi-subject ICA and dual regression. *NeuroImage, 47(Suppl 1)*:S148. doi: 10.1016/S1053-8119(09)71511-3

493 Behzadi Y, Restom K, Liau J, Liu TT (2007) A component based noise correction method (CompCor)
494 for BOLD and perfusion based fMRI. *NeuroImage, 37:*90-101. doi:
495 10.1016/j.neuroimage.2007.04.042
496 Bell PT, Shine JM (2015) Estimating large-scale network convergence in the human functional
497 connectome. *Brain Connectivity, 5:*565-574. doi: 10.1089/brain.2015.0348
498 Bell PT, Shine JM (2016) Subcortical contributions to large-scale network communication.
499 *Neuroscience and Biobehavioral Reviews, 71:*313-322. doi: 10.1016/j.neubiorev.2016.08.036
500 Bennarroch EE (2013) Pedunculopontine nucleus: Functional organization and clinical implications.
501 *Clinical Implications of Neuroscience Research, 80:*1148-1155. doi:
502 10.1212/WNL.0b013e3182886a76
503 Blessing EM, Beissner F, Schumann A, Brünner F, Bär K-J (2016) A data-driven approach to mapping
504 cortical and subcortical intrinsic functional connectivity along the longitudinal hippocampal axis.
505 *Human Brain Mapping, 37:*462-476. doi: 10.1002/hbm.23042
506 Braga RM, Sharp DJ, Leeson C, Wise RJS, Leech R (2013) Echoes of the brain within default mode,
507 association, and heteromodal cortices. *Journal of Neuroscience,* 28:14031-14039. doi:
508 10.1523/JNEUROSCI.0570-13.2013
509 Braga RM, Leech R (2015) Echoes of the brain: Local-scale representation of whole-brain functional
510 networks within transmodal cortex. *The Neuroscientist, 21:*540-551. doi:
511 10.1177/1073858415585730
512 Cheng H, Zhu H, Zheng Q, Liu J, He G (2020) Functional parcellation of the hippocampus by semi-
513 supervised clustering of resting state fMRI data. *Scientific Reports, 10:*16402. doi:
514 10.1038/s41598-020-73328-1
515 Cheng H, Liu J (2021) Concurrent brain parcellation and connectivity estimation via co-clustering of
516 resting state fMRI: A novel approach. *Human Brain Mapping, 42:*2477-2489. doi:
517 10.1002/hbm.25381

518 Choi EY, Yeo BTT, Buckner RL (2012) The organization of the human striatum estimated by intrinsic
519 functional connectivity. *Journal of Neurophysiology, 108:*2242-2263. doi: 10.1152/jn.00270.2012.
520 Costumero V, Bueichekú E, Adrián-Ventura J, Ávila C (2020) Opening or closing eues at rest
521 modulates the functional connectivity of V1 with default and salience networks. *Sci Reports,*
522 10:9137. doi: 10.1038/s41598-020-66100-y
523 Cox RW (1996) AFNI: software for analysis and visualization of functional magnetic resonance
524 neuroimages. *Comput Biomed Res*, 29:162-73. doi: 10.1006/cbmr.1996.0014
525 Damoiseaux JS, Rombouts SARB, Barkhof F, Scheltens P, Stam CJ, Smith SM, Beckmann CF (2006)
526 Consistent resting-state networks across healthy subjects. *PNAS, 103:*13848-13853. doi:
527 10.1073/pnas.0601417103
528 De Gee JW, Colizoli O, Kloosterman NA, Knapen T, Nieuwenhuis S, Donner TH (2017) Dynamic
529 modulation of decision biases by brainstem arousal systems. *eLife, 6*:e23232. doi:
530 10.7554/elife.23232
531 De Hollander G, Keuken MC, Forstmann BU (2015) The subcortical cocktail problem: Mixed signals
532 from the subthalamic nucleus and substantia nigra. *PLoS One, 10:*e0120572. doi:
533 10.1371/journal.pone.0120572
534 De Hollander G, Keuken MC, Van der Zwaag W, Forstmann BU, Trampel R (2017) Comparing
535 functional MRI protocols for small, iron-rich basal ganglia nuclei such as the subthalamic nucleus
536 at 7 T and 3 T. *Human Brain Mapping, 38:*3226-3248. doi: 10.1002/hbm.23586
537 Edlow BL (2021) Dopaminergic modulation of human consciousness via default mode network
538 connectivity. *PNAS, 118:*e2111268118. doi: 10.1073/pnas.2111268118.
539 Esteban O, Markiewicz CJ, Blair RW, Moodie CA, Isik AI, Erramuzpe A, Kent JD, Goncalves M, DuPre E,
540 Snyder M, Oya H, Ghosh SS, Wright J, Durnez J, Poldrack RA, Gorgolewski KJ (2018) fMRIPrep: a
541 robust preprocessing pipeline for functional MRI. *Nature Methods*, *16*:111-116. doi:
542 10.1038/s41592-018-0235-4

543 Ezama L, Hernández-Cabrera JA, Seoane S, Pereda E, Janssen N (2021) Functional connectivity of the
544 hippocampus and its subfields in resting-state networks. *European Journal of Neuroscience,*
545 *53:*3378-3393. doi: 10.1111/ejn.15213
546 Fonov VS, Evans AC, McKinstry RC, Almli CR, Collins DL (2009) Unbiased nonlinear average age-
547 appropriate brain templates from birth to adulthood. *NeuroImage, 47:*102. doi: 10.1016/S1053-
548 8119(09)70884-5
549 Forstmann BU, De Hollander G, Van Maanen L, Alkemade A, Keuken MC (2017) Towards a
550 mechanistic understanding of the human subcortex. *Nature Reviews, 18:*57-65. doi:
551 10.1038/nrn.2016.163
552 Frässle S, Aponte EA, Bollmann S, Brodersen KH, Do CT, Harrison OK, Harrison SJ, Heinzle J, Iglesias S,
553 Kasper L, Lokamina EI, Mathys C, Müller-Schrader M, Pereira I, Petzschner FH, Raman S, Schöbi D,
554 Toussaint B, Weber LA, Yao Y, Stephan KE (2021) TAPAS: an open-source software package for
555 Translational Neuromodeling and Computational Psychiatry. *Frontiers in Psychiatry, 12:*680811.
556 doi: 103389/fpsyt.2021.680811
557 Glover GH, Li TQ, Ress D (2000) Image-based method for retrospective correction of physiological
558 motion effects in fMRI: RETROICOR. *Magnetic Resonance in Medicine, 44:*162-167.
559 Gorgolewski K, Burns CD, Madison C, Clark D, Halchenko YO, Waskom ML, Ghosh SS (2011) Nipype: a
560 flexible, lightweight and extensible neuroimaging data processing framework in Python. *Frontiers*
561 *in Neuroinformatics*, 5:13. doi: 10.3389/fninf.2011.00013
562 Grayson DS, Ray S, Carpenter S, Iyer S, Costa Dias TG, Stevens C, Nigg JT, Fair DA (2014) Structural
563 and functional rich club organization of the brain in children and adults. *PloS One, 9:*e88297. Doi:
564 10.1371/journal.pone.0088297
565 Greene DJ, Marek S, Gordon EM, Siegel JS, Gratton C, Laumann TO, Gilmore AW, Berg JJ, Nguyen AL,
566 Dierker D, Van AN, Ortega M, Newbold DJ, Hampton JM, Nielsen AN, McDermott KB, Roland JL,
567 Norris SA, Nelson SM, Snyder AZ, Schlagger BL, Petersen SE, Dosenbach NUF (2020) Integrative

568 and network-specific connectivity of the basal ganglia and thalamus defined in individuals.
569 *Neuron, 105:*742-758. doi: 10.1016/j.neuron.2019.11.012
570 Greve DN, Fischl B (2009) Accurate and robust brain image alignment using boundary-based
571 registration. *NeuroImage, 48:*63-72. doi: 10.1016/j.neuroimage.2009.06.060
572 Groot JM, Csifcsák G, Wientjes S, Forstmann BU, Mittner M (2022) Catching wandering minds with
573 tapping fingers: Neural and behavioral insights into task-unrelated cognition. *Cerebral Cortex,* doi:
574 10.1093/cercor/bhab494
575 Haber SN (2003) The primate basal ganglia: Parallel and integrative networks. *Journal of Chemical*
576 *Neuroanatomy, 26:*317-330. doi: 10.1016/j.jchemneu.2003.10.003
577 Han J, Zhou L, Wu H, Huang Y, Qiu M, Huang L, Lee C, Lane TJ, Qin P (2023) Eyes-open and eyes-
578 closed resting state network connectivity differences. *Brain Sci,* 13:122. doi:
579 10.3390/brainsci13010122
580 Harrison OK, Guell X, Klein-Flügge MC, Barry RL (2021) Structural and resting state functional
581 connectivity beyond the cortex. *NeuroImage, 240:*118379. doi:
582 10.1016/j.neuroimage.2021.118379
583 Hu Y, Yang Z (2021) Impact of inter-individual variability on the estimation of default mode network
584 in temporal concatenation group ICA. *NeuroImage, 237:*118114. doi:
585 10.1016/j.neuroimage.2021.118114
586 Hwang K, Bertolero MA, Liu WB, D'Esposito M (2017) The human thalamus is an integrative hub for
587 functional brain networks. *J Neurosci, 37:*5594-5607
588 Jarbo K, Verstynen TD (2015) Converging structural and functional connectivity of orbitofrontal,
589 dorsolateral, prefrontal, and posterior parietal cortex in the human striatum. *J Neurosci, 35:*3865-
590 3878. doi: 10.1523/JNEUROSCI.2636-14.2015
591 Jenkinson M, Bannister P, Brady JM, Smith SM (2002) Improved optimisation for the robust and
592 accurate linear registration and motion correction of brain images. *NeuroImage*, 17:825-841. doi:
593 10.1016/s1053-8119(02)91132-8

Jenkinson M, Smith SM (2001) A global optimisation method for robust affine registration of brain images. *Medical Image Analysis*, 5:143-156. doi: 10.1016/s1361-8415(01)00036-6

Ji JL, Spronk M, Kulkarni K, Repovs G, Anticevic A, Cole MW (2019) Mapping the human brain's cortical-subcortical functional network organization. *NeuroImage, 185:*35-57. doi: 10.1016/j.neuroimage.2018.10.006

Kasper L, Bollmann S, Diaconescu AO, Hutton C, Heinzle J, Iglesias S, Hauser TU, Sebold M, Manjaly Z-M, Pruessmann KP, Stephan KE (2017) The PhysIO Toolbox for modeling physiological noise in fMRI data. *Journal of Neuroscience Methods, 276*: 56-72. doi: 10.1016/j.jneumeth.2016.10.019

Kerestes R, Chase HW, Philips ML, Ladouceur CD, Eickhoff SB (2017) Multimodal evaluation of the amygdala's functional connectivity. *NeuroImage, 148:*219-229. doi: 10.1016/j.neuroimage.2016.12.023

Keuken MC, Isaacs BR, Trampel R, Van der Zwaag W, Forstmann BU (2018) Visualizing the human subcortex using ultra-high field magnetic resonance imaging. *Brain Topography, 31:*513-545. doi: 10.1007/s10548-018-0638-7

Krimmel SR, White MG, Panicker MH, Barrett FS, Mathur BN, Seminowicz DA (2019) Resting state functional connectivity and cognitive task-related activation of the human claustrum. *NeuroImage, 196:*59-67. doi: 10.1016/j.neuroimage.2019.03.075

Lee T-W, Xue S-W (2018) Functional connectivity maps based on hippocampal and thalamic dynamics may account for the default-mode network. *European Journal of Neuroscience, 47:*388-398. doi: 10.1111/ejn.13828

Lee WH, Moser DA, Ing A, Doucet GE, Frangou S (2019) Behavioral and health correlates of resting-state metastability in the Human Connectome Project. *Brain Topography, 32:*80-86. doi: 10.1007/s10548-018-0672-5

Leech R, Braga R, Sharp DJ (2012) Echoes of the brain within the posterior cingulate cortex. *Journal of Neuroscience, 32:*215-222. doi: 10.1523/JNEUROSCI.3689-11.2012

619 Li J, Curley WH, Guerin B, Dougherty DD, Dalca AV, Fischl B, Horn A, Edlow BL (2021) Mapping the
620 subcortical connectivity of the human default mode network. *NeuroImage, 245*:118758. doi:
621 10.1016/j.neuroimage.2021.118758
622 Liégeois R, Li J, Kong R, Orban C, Van de Ville D, Ge T, Sabuncu MR, Yeo T (2019) Resting brain
623 dynamics at different timescales capture distinct aspects of human behavior. *Nature*
624 *Communications, 10:*2317. doi: 10.1038/s41467-019-10317-7
625 Liu KY, Marijatta F, Hämmerer D, Acosta-Cabronero J, Düzel E, Howard RJ (2017) Magnetic resonance
626 imaging of the human locus coeruleus: A systematic review. *Neuroscience and Biobehavioral*
627 *Reviews, 83:*325-355. doi: 10.1016/j.neubiorev.2017.10.023
628 Lyu D, Pappas I, Menon DK, Stamatakis EA (2021) A precuneal causal loop mediates external and
629 internal information integration in the human brain. *Journal of Neuroscience, 41:*9944-9956. doi:
630 10.1523/JNEUROSCI.0647-21.2021
631 Marek S, Greene DJ (2021) Precision functional mapping of the subcortex and cerebellum. *Current*
632 *Opinion in Behavioral Sciences, 40:*12-18. doi: 10.1016/j.cobeha.2020.12.011
633 Martinez-Gonzales C, Bolam JP, Mena-Segovia J (2011) Topographical organization of the
634 pedunculopontine nucleus. *Frontiers in Neuroanatomy, 5:*22. doi: 10.3389/fnana.2011.00022
635 Marques JP, Kober T, Krueger G, Van der Zwaag W, Van de Moortele PF, Gruetter R (2010) MP2RAGE,
636 a self bias-field corrected sequence for improved segmentation and T1-mapping at high field.
637 *NeuroImage, 15*:1271-81. doi: 10.1016/j.neuroimage.2009.10.002
638 Miletic S, Bazin P-L, Weiskopf N, Van der Zwaag W, Forstmann BU, Trampel R (2020) fMRI protocol
639 optimization for simultanously studying small subcortical and cortical areas at 7 T. *NeuroImage,*
640 *219:*116992. doi: 10.1016/j.neuroimage.2020.116992
641 Mittner M, Hawkins GE, Boekel W, Forstmann BU (2016) A neural model of mind wandering. *Trends*
642 *in Cognitive Sciences*, 20:570-578. doi: 10.1016/j.tics.2016.06.004

643 Munn BR, Müller EJ, Wainstein G, Shine JM (2021) The ascending arousal system shapes neural
644 dynamics to mediate awareness of cognitive states. *Nat Comm, 12:*6016. doi: 10.1038/s41467-
645 021-26268-x
646 O'Callaghan C, Walpola IC, Shine JM (2020) Neuromodulation of the mind-wandering brain state: The
647 interaction between neuromodulatory tone, sharp wave-ripples and spontaneous thought.
648 *Philosophical Transactions of the Royal Society, 376:*20190699. doi: 10.1098/rstb.2019.0699
649 Odekerken VJJ, Van Laar T, Staal MJ, Mosch A, Hoffmann CFE, Nijssen PCG, Beute GN, Van Vugt JPP,
650 Lenders MWPM, Contarino MF, Mink MSJ, Bour LJ, Van den Munckhof P, Schmand BA, De Haan
651 RJ, Schuurman PR, De Bie RMA (2013) Subthalamic nucleus versus globus pallidus bilateral deep
652 brain stimulation for advanced Parkinson's disease (NSTAPS study): A randomised controlled trial.
653 *The Lancet Neurology, 12:*37-44. https://doi.org/10.1016/S1474-4422(12)70264-8
654 Qin S, Duan X, Supekar K, Chen H, Chen T, Menon V (2016) Large-scale intrinsic functional network
655 organization along the long axis of the human medial temporal lobe. *Brain Structure and Function,*
656 *221:*3237-3258. doi: 10.1007/s00429-015-1098-4
657 Seitzman BA, Gratton C, Marek S, Raut RV, Dosenbach NUF, Schlagger BL, Petersen SE, Greene DJ
658 (2020) A set of functionally-defined brain regions with improved representation of the subcortex
659 and cerebellum. *NeuroImage, 206:*116290. doi: 10.1016/j.neuroimage.2019.116290
660 Senden M, Deco G, De Reus MA, Goebel R, Van den Heuvel MP (2014) Rich club organization
661 supports a diverse set of functional network configurations. *NeuroImage, 96:*174-182. doi:
662 10.1016/j.neuroimage.2014.03.066
663 Seoane S, Modroño C, Gonzáles-Mora J, Janssen N (2022) Medial temporal lobe contributions to
664 resting-state networks. *Brain Structure and Function, 227:*995-1012. doi: 10.1007/s00429-021-
665 02442-1
666 Singh K, Cuazzo S, García-Gomar MG, Stauder M, Vanello N, Passino C, Bianciardi M (2022) Functional
667 connectome of arousal and motor brainstem nuclei in living humans by 7 Tesla resting-state fMRI.
668 *NeuroImage, 249:*118865. doi: 10.1016/j.neuroimage.2021.118865

669 Smith JB, Lee AK, Jackson J (2020) The claustrum. *Current Biology, 30:*1401-1406. doi:
670 10.1016/j.cub.2020.09.069
671 Smith SM, Brady JM (1997) SUSAN – a new approach to low level image processing. *Int J Comput Vis*,
672 23:45-78. doi: 10.1023/A:1007963824710
673 Sylvester CM, Yu Q, Srivastava AB, Marek S, Zheng A, Alexopoulos D, Smyser CD, Shimony JS, Ortega
674 M, Dierker DL, Patel GH, Nelson SM, Gilmore AW, McDermott KB, Berg JJ, Drysdale AT, Perino MT,
675 Snyder AZ, Raut RV, Laumann TO, Gordon EM, Barch DM, Rogers CE, Greene DJ, Raichle ME,
676 Dosenbach NUF (2020) Individual-specific functional connectivity of the amygdala: A substrate for
677 precision psychiatry. *PNAS, 117:*3808-3818. doi: 10.1073/pnas.1910842117
678 Tian Y, Margulies DS, Breakspear M, Zalesky A (2020) Topographic organization of the human
679 subcortex unveiled with functional connectivity gradients. *Nature Neuroscience, 23:*1421-1432.
680 doi: 10.1038/s41593-020-00711-6
681 Tomasi D, Volkow ND (2011) Association between functional connectivity hubs and brain networks.
682 *Cerebral Cortex, 21:*2003-2013. doi: 10.1093/cercor/bhq268
683 Tustison NJ, Avants BB, Cook PA, Zheng Y, Egan A, Yushkevich PA (2010) N4ITK: improved N3 bias
684 correction. *IEEE Trans Med Imaging*, 29:1310-1320. doi: 10.1109/TMI.2010.2046908
685 Van der Heuvel MP, Sporns O (2011) Rich-club organization of the human connectome. *Journal of*
686 *Neuroscience, 31:*15775-15786. doi: 10.1523/JNEUROSCI.3539-11.2011
687 Varoquaux G, Sadaghiani S, Pinel P, Kleinschmidt A, Poline JB, Thirion B (2010) A group model for
688 stable multi-subject ICA from fMRI datasets. *NeuroImage, 51:*288-299. doi:
689 10.1016/j.neuroimage.2010.02.010
690 Woolrich MW, Ripley BD, Brady M, Smith SM (2001) Temporal autocorrelation in univariate linear
691 modeling of FMRI data. *NeuroImage,* 14:1370-1386. doi: 10.1006/nimg.2001.0931
692 Ye R, Rua C, O'Callaghan C, Jones PS, Hezemans FH, Kaalund SS, Tsvetanov KA, Rodgers CT, Williams
693 G, Passamonti L, Rowe JB (2021) An *in vivo* probabilistic atlas of the human locus coeruleus at
694 ultra-high field. *NeuroImage, 225:*117487. doi: 10.1016/j.neuroimage.2020.117487

695 BTT, Krienen FM, Sepulcre J, Sabuncu MR, Lashkari D, Hollinshead M, Roffman JL, Smoller JW, Zöllei
696 L, Polimeni JR, Fischl B, Liu H, Buckner RL (2011) The organization of the human cerebral cortex
697 estimated by intrinsic functional connectivity. *Journal of Neurophysiology*, 106:1125-1165. doi:
698 10.1152/jn.00338.2011
699 Zarzycki MZ, Domitrz I (2020) Stimulation-induced side effects after deep brain stimulation – a
700 systematic review. *Acta Neuropsychiatrica, 32*:57–64. doi: 10.1017/neu.2019.35
701 Zhang Y, Brady M, Smith S (2001) Segmentation of brain MR images through a hidden markov
702 random field model and the expectation-maximization algorithm. *IEEE Trans Med Imag*, 20:45-57.
703 doi: 10.1109/42.906.424
704 Zhang S, Hu S, Chao HH, Li C-SR (2016) Resting-state functional connectivity of the locus coeruleus in
705 humans: In comparison with the ventral tegmental area/substantia nigra pars compacta and the
706 effects of age. *Cerebral Cortex, 26:*3413-3427. doi: 10.1093/cercor/bhv172
707 Zuberer A, Kucyi A, Yamashita A, Wu CM, Walter M, Valera EM, Esterman M (2021) Integration and
708 segregation across large-scale intrinsic brain networks as a marker of sustained attention and
709 task-unrelated thought. *NeuroImage*, 229:117610. doi: 10.1016/j.neuroimage.2020.117610
710 Zuo X-N, Kelly C, Adelstein JS, Klein DF, Castellanos FX, Milham MP (2010) Reliable intrinsic
711 connectivity networks: Test-retest evaluation using ICA and dual regression approach.
712 *NeuroImage, 49:*2163-2177. doi: 10.1016/j.neuroimage.2009.10.080

Figure/Table legends

Figure 1. Overview of the data analysis.

Figure 2. Parcellations of subcortical regions of interest and reference networks. (a) Subcortical regions of interest defined with open-source atlases and **(b)** data-driven reference networks from a whole-brain canonical ICA on the resting-state timeseries, labeled according to their maximum spatial correlation with a 17-network cortical parcellation. Corresponding whole-brain tSNR maps are shown in Figure 2-1. *Labels: thalamus (Tha), striatum (Str), globus pallidus externa (GPe), globus pallidus interna (GPi), claustrum (Cl), hippocampus (HPC), amygdala (Amg), substantia nigra (SN), subthalamic nucleus (STN), ventral tegmental area (VTA), red nucleus (RN), periaqueductal grey (PAG), pedunculopontine nucleus (PPN), locus coeruleus (LC), Somatomotor A/B (SomA/B), Control A/B/C (ConA/B/C), Temporal Parietal (TemPar), Dorsal Attention A/B (DorA/B), Default A/B (DefA/B), Visual Central (VisC), Visual Peripheral (VisP), Limbic A/B (LimA/B), Salience/Ventral Attention A/B (SalA/B).*

Figure 3. Echoes of intrinsic connectivity networks in the subcortex. (a) The number of distinct subregions within a ROI with a functional connectivity profile that resembled a reference network ('Subregions') and the number of different reference networks that were echoed within a region ('Networks') both defined by counting above-threshold spatial correlations. **(b)** The maximum spatial correlation between each ROI and each reference network, independent of subregion, for nine ROIs that demonstrated at least one above-threshold spatial correlation to any reference network. Subregional connectivity profiles for a subset of structures and their spatial correlation with reference networks are illustrated in Figure 3-1. The same analysis was repeated with reference networks taken from the 17-network cortical parcellation (Yeo et al 2011) shown in Figure 3-2 as well as for three cortical ROIs (Figure 3-3). *Labels: thalamus (Tha), striatum (Str), globus pallidus externa (GPe), claustrum (Cl), hippocampus (HPC), amygdala (Amg), substantia nigra (SN), ventral tegmental area (VTA), pedunculopontine nucleus (PPN), Somatomotor A (SomA), Somatomotor B (SomB), Control A (ConA), Control B (ConB), Control C (ConC), Temporal Parietal (TemPar), Dorsal Attention A (DorA), Dorsal Attention B (DorB), Default A (DefA), Default B (DefB), Visual Central (VisC), Visual Peripheral (VisP), Limbic A (LimA), Limbic B (LimB), Salience/Ventral Attention A (SalA), Salience/Ventral Attention B (SalB).*

Figure 4. Topography of network echoes within heteromodal subcortical structures. Spatiotemporal decomposition of subcortical structures into independent subregions, color coded according to their strongest network echo or made translucent if their maximum spatial correlation with any reference network did not reach threshold. *Labels: thalamus (Tha), striatum (Str), globus pallidus externa (GPe), claustrum (Cl), hippocampus (HPC), substantia nigra (SN), ventral tegmental area (VTA), Somatomotor A (SomA), Somatomotor B (SomB), Control A (ConA), Control B (ConB), Control C (ConC), Temporal Parietal (TemPar), Dorsal Attention A (DorA), Dorsal Attention B (DorB), Default A (DefA), Default B (DefB), Visual Central (VisC), Visual Peripheral (VisP), Limbic A (LimA), Limbic B (LimB), Salience/Ventral Attention A (SalA), Salience/Ventral Attention B (SalB).*

Figure 2-1. Whole-brain temporal signal to noise ratio (tSNR). For each of the two fMRI runs, voxel-wise tSNR values were calculated as the ratio of the mean and standard deviation of the resting-state timeseries after temporal high-pass filtering (1/128s) to remove low-frequency signal drifts. Individual tSNR maps (n=40) were registered to standard MNI space (MNI152NIin2009cAsym) with ANTs before voxel-wise tSNR values were averaged across subjects and runs to create the group-level map. The black contours outline the regions of interest that were included in the study.

Figure 3-1. Functional connectivity patterns of subcortical subregions and their spatial overlap with intrinsic connectivity networks. Diversity in whole-brain functional connectivity (FC) of distinct subregions of subcortical structures plotted on cortical surface meshes and the maximum spatial correlation with data-driven reference networks (four out of sixteen networks shown for illustration). Although the spatial correlations are

calculated from the unthresholded spatial maps, the reference networks were thresholded by assigning each voxel to its most strongly associated network based on the group canICA (i.e., every voxel is assigned to only one network and networks are non-overlapping) for illustration purposes. The subregion-specific FC maps are the group-level results of a dual regression analysis on the timecourse for each subregion while controlling for the variance in the other subregions, statistically tested with random permutation testing and thresholded at $p<.05$. *Labels: thalamus (Tha), striatum (Str), claustrum (Cl), hippocampus (HPC), subsantia nigra (SN), globus pallidus externa (GPe), Default A (DefA), Default B (DefB), Somatomotor A (SomA), Salience/Ventral Attention A (SalA).*

Figure 3-2. Echoes of well-established cortical intrinsic connectivity networks in the subcortex. (a) The number of distinct subregions within a region of interest (ROI) with a functional connectivity profile that resembled a reference network ('Subregions') and the number of different reference networks that were echoed within a region ('Networks') both counted as the number of above-threshold spatial correlations. Reference networks were taken from the 17-network cortical parcellation (Yeo et al 2011). **(b)** The maximum spatial correlation between each ROI and each reference network, independent of subregion, for nine ROIs that demonstrated at least one above-threshold spatial correlation. *Labels: thalamus (Tha), striatum (Str), globus pallidus externa (GPe), claustrum (Cl), hippocampus (HPC), amygdala (Amg), substantia nigra (SN), ventral tegmental area (VTA), pedunculopontine nucleus (PPN), Somatomotor A (SomA), Somatomotor B (SomB), Control A (ConA), Control B (ConB), Control C (ConC), Temporal Parietal (TemPar), Dorsal Attention A (DorA), Dorsal Attention B (DorB), Default A (DefA), Default B (DefB), Default C (DefC), Visual Central (VisC), Visual Peripheral (VisP), Limbic A (LimA), Limbic B (LimB), Salience/Ventral Attention A (SalA), Salience/Ventral Attention B (SalB).*

Figure 3-3. Echoes of intrinsic connectivity networks in cortical regions of interest. (a) The maximum spatial correlation between the whole-brain functional connectivity (FC) of each cortical ROI with data-driven reference networks. The results demonstrate greater functional heterogeneity within posterior cingulate cortex (PCC) and medial prefrontal cortex (mPFC), as evident in more distributed patterns of FC with default mode, control, and salience networks compared to the visual cortex (VC), which showed a more uniform organization dominated by a preferential connection with the visual peripheral network. This is consistent with previous work (Braga et al 2013) and provides a validation for our novel application of the multivariate analysis within subcortical regions of interest. **(b)** The results of an identical analysis but with the 17-network cortical parcellation (Yeo et al 2011) as reference networks, revealing a less pronounced but qualitatively similar pattern of results compared to the data-driven networks. *Labels: Somatomotor A (SomA), Somatomotor B (SomB), Control A (ConA), Control B (ConB), Control C (ConC), Temporal Parietal (TemPar), Dorsal Attention A (DorA), Dorsal Attention B (DorB), Default A (DefA), Default B (DefB), Default C (DefC), Visual Central (VisC), Visual Peripheral (VisP), Limbic A (LimA), Limbic B (LimB), Salience/Ventral Attention A (SalA), Salience/Ventral Attention B (SalB).*

Table 1. Parcellationd details for regions of interest. Number of voxels (*N* voxels) in functional space (1.5mm isotropic voxel size) and mean and standard deviation (SD) of ROI-wise temporal signal-to-noise ratio (tSNR) values. *Source: Multi-contrast Anatomical Subcortical Parcellation (MASSP, Bazin et al 2020); 17-network cortical parcellation (Yeo et al 2011); 7T Probabilistic LC Atlas (Ye et al 2021).

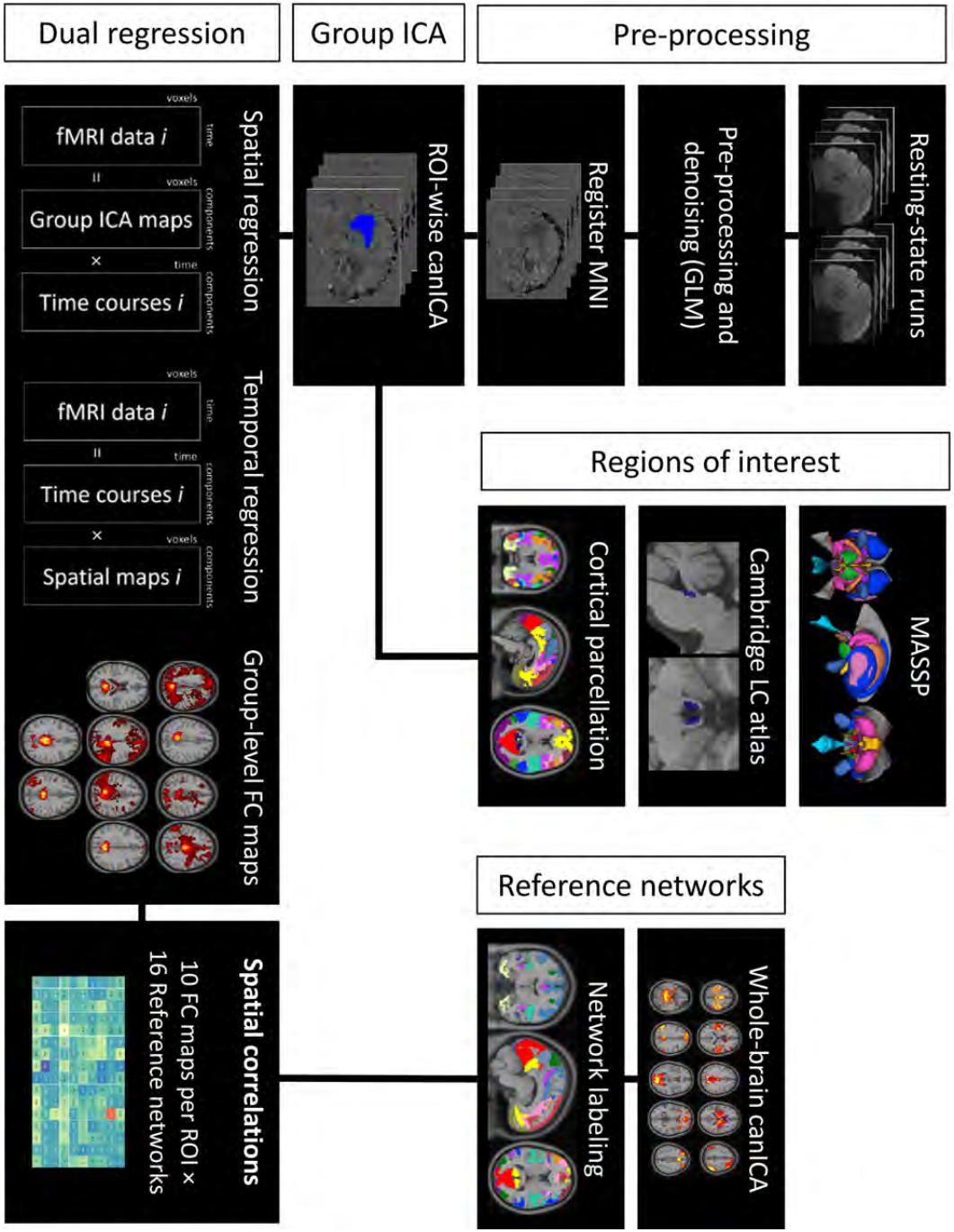
Dual regression
Group ICA
Pre-processing
Resting-state runs
Pre-processing and denoising (GLM)
Register MNI
ROI-wise canICA
Regions of interest
MASSP
Cambridge LC atlas
Cortical parcellation
Reference networks
Whole-brain canICA
Network labeling
Spatial regression
fMRI data i
Group ICA maps
Time courses i
Temporal regression
fMRI data i
Time courses i
Spatial maps i
Group-level FC maps
Spatial correlations
10 FC maps per ROI x
16 Reference networks